

# Multipath assisted positioning with arbitrary wall shapes using Doppler information

Benedikt J. Müller, Martin Schmidhammer, Michael Walter, Christian Gentner, Siwei Zhang, Armin Dammann *Institute of Communications and Navigation, German Aerospace Center (DLR)*, 82234 Weßling, Germany {benedikt.mueller, martin.schmidhammer, m.walter, christian.gentner, siwei.zhang, armin.dammann}@dlr.de

Abstract—This paper presents an algorithm that exploits multipath propagation for the position estimation of mobile receivers. The proposed method utilizes two pieces of information of this multipath signal component: First the delay and thus the path length restricting possible reflection points to an ellipse. And second the Doppler shift of this multipath component to infer angular information along this ellipse. By exploiting relative Doppler information, obtained from the phase difference between the line-of-sight path and multipath components, the approach eliminates the need for strict synchronization requirements. In contrast to state-of-the-art methods that rely on the concept of static virtual transmitters and assume idealized straight wall geometries, the proposed algorithm directly estimates the positions of reflection points. The direct estimation of reflection points allows simultaneous localization and mapping of environments with arbitrary wall shapes. The feasibility of the approach is demonstrated through simulations incorporating delay and Doppler measurements of multipath components. Results confirm that the method enables accurate estimation of both receiver position and reflection points for a variety of wall geometries, including convex and concave surfaces.

Index Terms—SLAM, swarm navigation, Doppler, multipath propagation, MPC, relative Doppler, reflection point, Channel-SLAM, curved wall, single antenna AoA

#### I. Introduction

In wireless communication systems, transmitted signals often encounter multipath propagation, where they are reflected, diffracted, or scattered by surrounding objects. As a result, the signal received by an antenna typically comprises multiple delayed copies of the original transmission, commonly known as multipath components (MPCs). In recent years, multipath assisted positioning approaches became widely used, exploiting MPCs for positioning instead of mitigating them. The authors in [1]–[3] treat MPCs as line-of-sight (LoS) signals from virtual transmitters (VTs) which are assumed to be static during the movement of the receiver. Especially, with Channel-SLAM, an algorithm was introduced which estimates simultaneously the positions of the receiver and the VTs based on the estimated parameters of the MPCs using a simultaneous localization and mapping (SLAM) approach.

Several studies have also explored the use of MPCs to estimate the positions of reflecting surfaces such as walls [1], [4], [5]. These methods predominantly use time of flight (ToF) measurements of MPCs for mapping walls, whereby ToF information confine the location of the corresponding reflection point (RP) to an ellipse [6]. However, the exact position along the ellipse cannot be determined solely from

ToF information but needs to be resolved through successive measurements in a dynamic system.

In order to enhance mapping capabilities, we propose to consider an additional measurement, different from ToF, that provides angular information to help localize the RP along the ellipse. Possible sources of this additional information are angle of arrival (AoA), Doppler shift, and differential distance, defined as the change in path length over consecutive timesteps. Measuring AoA requires an antenna array with at least two elements [7], whereas Doppler shift and differential distance can be derived using a single omnidirectional antenna, provided that the system is in motion. Using these measurements, the vector between the RP, transmitter (Tx) and receiver (Rx) can determined, allowing to infer angular information [8]. For the Doppler measurement, a phase-coherent Tx-Rx pair is necessary, but this is challenging with low-cost and thus scalable swarm hardware, such as ultra-wideband (UWB) based systems [6]. To avoid the need for strict synchronization, our approach uses relative Doppler measurements, derived from the phase difference between LoS and MPC in the received signal. Note that relative Doppler measurements are also used for passive bistatic radar (PBR), where an uncooperative Tx is used as an illuminator [9]. Compared to [1], we propose a single antenna SLAM algorithm that directly maps the locations of RPs and does explicitly not rely on the concept of VTs. The proposed algorithm is thus applicable to not only flat but arbitrary wall shapes. While flat walls can be assumed for idealized buildings, naturally formed environments such as caves or cluttered indoor spaces have more complex structure. The ability to account for such structures becomes particularly relevant when deploying robotic swarms for exploration in unknown environments.

The algorithm is validated through simulations involving a mobile node navigating along walls of varying shapes: straight, convex, concave, and kinked; using only two static anchors. These scenarios test the algorithm's ability to simultaneously track the mobile position and estimate RPs on walls using ToF and Doppler measurements. Key results show that the method enables SLAM even with non-linear wall geometries and single-antenna setups, with reliable mobile tracking and acceptable RP estimation accuracy. Notably, Doppler information helps resolve angular ambiguity on MPC ellipses, and concave walls allow faster mapping due to better geometric alignment.

The remainder of the paper is organized as follows: Section

II presents the system model and estimation method; Section III details the simulation setup and results; Section IV concludes the paper with key findings and future work.

#### II. METHOD

In this section we define the general system geometry, the states of the system and the transition model, which describes how these states evolve over time. Further we introduce a measurement model and an estimator using the measurement result as well as the transition and measurement model.

## A. State model

Consider a two-dimensional system containing static anchor nodes and dynamic mobile nodes. Next consider the system to additionally include walls which can reflect signals that are sent between nodes. Each RP on the wall is characteristic for a first order reflection and thus a specific MPC in the signal propagated between a Tx and Rx node pair. Higher order reflections will be neglected in this work assuming they can be filtered out due to sufficiently low signal strength [4]. In this work, the position of the anchors is known and all other positions are treated as unknown, thus requiring localization.

Let  $\mathcal{M}$ ,  $\mathcal{A}$  and  $\mathcal{R}$  be the set of all mobiles, anchors and reflection points. Then M, A and R define the cardinality of these sets. These quantities might change with time for example due to the visibility between nodes or the (dis)appearance of reflection points.

We define the state of a mobile or an anchor  $x_i$ ,  $i \in \mathcal{M} \cup \mathcal{A}$  to include position  $p_i = [x_i, y_i]^\top$  and velocity  $\dot{p}_i = [\dot{x}_i, \dot{y}_i]^\top$ ,

$$\boldsymbol{x}_i = [x_i, \dot{x}_i, y_i, \dot{y}_i]^\top. \tag{1}$$

The state of the reflection point  $x_r$ ,  $r \in \mathcal{R}$ , is defined as,

$$\boldsymbol{x}_r = [x_r, y_r]^\top = \boldsymbol{p}_r, \tag{2}$$

only including its position, since we do not want to infer anything about its dynamic behavior. In a more complex system description, this dynamic could be modeled, by extending the state vector to include the velocity of the reflection point or the normal vector of the wall at this point. Every RP  $r \in \mathcal{R}$  is generated by the signal between nodes i and j that is reflected by a wall, so there is a direct function  $f \colon \mathcal{R} \to \{\{i,j\}|i,j\in\mathcal{A}\cup\mathcal{M}\}$ . Note that depending on the wall shape and the geometry of the system there might be multiple reflection points  $\{r_1,r_2\} \subset \mathcal{R}$  with  $f(r_1) = f(r_2)$ .

Assembling all unknown quantities into one state vector s, we get

$$\boldsymbol{s} = \left[ \left( \boldsymbol{x}_i^{\top} \right)_{i \in \mathcal{M} \cup \mathcal{R}} \right]^{\top} . \tag{3}$$

This state vector evolves over time. We denote  $s_k$  the state vector at snapshot  $k \in \mathbb{N}$  and time  $t_k$ , where  $t_{k+1} > t_k$ . Further we define the time increment between two snapshots as  $\Delta t_k = t_{k+1} - t_k$ . As a state transition model we use the constant velocity model [10] for mobiles and a more simple

random walk model for the RP. Following these models, we define the transition matrices as

$$\boldsymbol{F}_{i}(\Delta t) = \begin{bmatrix} 1 & \Delta t & 0 & 0 \\ 0 & 1 & 0 & 0 \\ 0 & 0 & 1 & \Delta t \\ 0 & 0 & 0 & 1 \end{bmatrix}, \quad i \in \mathcal{M},$$
 (4)

$$\mathbf{F}_r(\Delta t) = \begin{bmatrix} 1 & 0 \\ 0 & 1 \end{bmatrix}, \quad r \in \mathcal{R},$$
 (5)

$$\mathbf{F}_{k} = \text{blkdiag}((\mathbf{F}_{i}(\Delta t_{k}))_{i \in \mathcal{M} \cup \mathcal{R}}), \quad k \in \mathbb{N}.$$
 (6)

Similar we define the process noise covariance matrices,

$$Q_{i}(\Delta t) = \sigma_{i}^{2} \begin{bmatrix} \frac{\Delta t^{3}}{3} & \frac{\Delta t^{2}}{2} & 0 & 0\\ \frac{\Delta t^{2}}{2} & \Delta t & 0 & 0\\ 0 & 0 & \frac{\Delta t^{3}}{3} & \frac{\Delta t^{2}}{2}\\ 0 & 0 & \frac{\Delta t^{2}}{2} & \Delta t \end{bmatrix}, \quad i \in \mathcal{M}, \quad (7)$$

$$Q_r(\Delta t) = \sigma_r^2 \begin{bmatrix} \Delta t & 0 \\ 0 & \Delta t \end{bmatrix}, \quad r \in \mathcal{R},$$
 (8)

$$\mathbf{Q}_{k} = \text{blkdiag}((\mathbf{Q}_{i}(\Delta t_{k}))_{i \in \mathcal{M} \cup \mathcal{R}}), \quad k \in \mathbb{N}, \quad (9)$$

with the respective process noise variances  $\sigma_i^2$  and  $\sigma_r^2$ , where the dependency on  $\Delta t$  has been factored out. Bringing everything together, we can define the fused state transition model,

$$s_{k+1} = F_k s_k + \eta_k$$
,  $\eta_k \sim \mathcal{N}(0, Q_k)$ . (10)

## B. Measurement model

In this work we will use two types of measurements, ToF to measure distances and Doppler measurements to infer information on the velocity along the propagation path. In the measurement model we will assume that distance and velocity is measured directly, a more detailed measurement procedure is not modeled. Note that the states of anchors, mobiles and RPs have a different number of components, but for ease of notation, we introduced the position  $\boldsymbol{p}$  and velocity states  $\dot{\boldsymbol{p}}$  as partial information of the full states  $\boldsymbol{x}$ . With this we can define the distance,

$$d_{ij} = d_{ji} = \sqrt{(x_i - x_j)^2 + (y_i - y_j)^2} = \|\boldsymbol{p}_i - \boldsymbol{p}_j\|,$$
 (11)

between two positions  $p_{\{i,j\}}$  with  $i,j \in \mathcal{A} \cup \mathcal{M} \cup \mathcal{R}$ . The length of a (first order) multipath is analogously defined as  $d_{irj} = d_{ir} + d_{rj}$ , with  $i,j \in \mathcal{A} \cup \mathcal{M}$  and  $r \in \mathcal{R}$ .

A Doppler shift in any wave system is observed when the propagation path length changes while the signal is transmitted or received. Specifically, the velocity component parallel to the propagation path, the projected velocity,

$$\Delta v_{ij} = \frac{\boldsymbol{p}_j - \boldsymbol{p}_i}{\|\boldsymbol{p}_i - \boldsymbol{p}_j\|} \cdot (\dot{\boldsymbol{p}}_i - \dot{\boldsymbol{p}}_j) , \qquad (12)$$

with  $i, j \in \mathcal{A} \cup \mathcal{M} \cup \mathcal{R}$ , is generating the Doppler frequency shift

$$\Delta f_{ij} = f_{\rm c} \, \frac{\Delta v_{ij}}{c} \,, \tag{13}$$

with the carrier frequency  $f_c$  and the speed of light c. Since the latter two are constants in our system, we will use  $\Delta v$ 

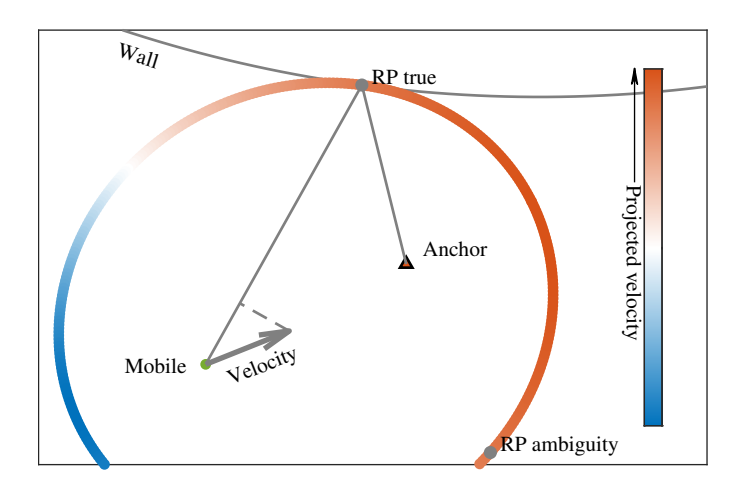


Fig. 1. This scheme illustrates the relation between a projected velocity, measurable as a Doppler shift in the signal, to the angular location on the ellipse formed by possible RPs with equidistant MPC. Note that this information is ambiguous and multiple RPs are possible for one projected velocity value.

instead of  $\Delta f$ , to define the Doppler measurement since then the numeric orders of all measurements are similar, and the notation is simplified.

Extending the definition of the LoS Doppler shift, we can derive the Doppler shift of a MPC,

$$\Delta v_{irj} = \Delta v_{ir} + \Delta v_{rj} \,, \tag{14}$$

with  $i, j \in A \cup M$  and  $r \in R$ , which becomes

$$\Delta v_{irj} = \frac{(\boldsymbol{p}_r - \boldsymbol{p}_i) \cdot \dot{\boldsymbol{p}}_i}{d_{ir}} + \frac{(\boldsymbol{p}_r - \boldsymbol{p}_j) \cdot \dot{\boldsymbol{p}}_j}{d_{jr}}, \quad (15)$$

for static reflectors such as walls in this case. In Fig. 1, such a projection is shown for a MPC, essentially providing information about the angular location of the RP on the ellipse formed by the propagation length of the MPC.

Since our system uses low-cost UWB chips for communication and navigation, the Tx and Rx clocks or, more specifically, their phase-locked loops are not synchronized. This makes it very challenging to observe Doppler in the direct and classical fashion, since this requires phase stability to integrate snapshot measurements over an extended time period. In this work, we introduce a new method of synchronization and thus Doppler measurement to the indoor navigation challenge. If both the MPC and the LoS component are recorded in the same channel impulse response (CIR), then their relative phase is stable because the synchronization offset between Tx and Rx is the same within one CIR. Using this, we are able to track their phase difference and extending on that, their relative Doppler shift,

$$\Delta \tilde{v}_{irj} = \Delta v_{irj} - \Delta v_{ij}$$
  
=  $\Delta v_{ir} + \Delta v_{rj} - \Delta v_{ij}$ , (16)

with  $i, j \in A \cup M$  and  $r \in R$ . Note that this method is used similarly in PBR scenarios where, due to signal strength restrictions, usually multiple antennas are used [9]. In an

indoor navigation scenario, the signal strength of the MPCs is stronger due to shorter propagation paths, and thus they are detectable in the same CIR as the LoS component [1], [11], [12].

Combining the above we can define the measurement function

$$\boldsymbol{H}(\boldsymbol{s}) := \boldsymbol{H}(\boldsymbol{s}; (\boldsymbol{x}_i)_{i \in \mathcal{A}}) = \left[ (d_{ij})_{i \in \mathcal{M}, j \in \mathcal{A} \cup \mathcal{M}, i < j \text{ if } j \in \mathcal{M}}, (d_{irj}, v_{irj})_{i \in \mathcal{M}, r \in \mathcal{R}, j \in \mathcal{A} \cup \mathcal{M}, i < j \text{ if } j \in \mathcal{M}} \right]^{\top},$$

$$(17)$$

dropping the argument for the dependency on the anchor state in the following. Next, we define the measurement model for the measurement  $z_k$  at snapshot k,

$$z_k = H(s_k) + \mu_k, \quad \mu_k \sim \mathcal{N}(0, \Sigma),$$
 (18)

with the noise value  $\mu_k$  drawn from a normal distribution with covariance matrix  $\Sigma$ . We assume that the measurements are uncorrelated at one snapshot, uncorrelated in time and independent of time and define the covariance matrix,

$$\Sigma = \operatorname{diag}\left(\left(\sigma_{\operatorname{dist}}^{2}\right)_{i \in \mathcal{M}, j \in \mathcal{A} \cup \mathcal{M}, i < j \text{ if } j \in \mathcal{M}},\right.$$

$$\left(\sigma_{\operatorname{dist}}^{2}, \sigma_{\operatorname{vel}}^{2}\right)_{i \in \mathcal{M}, r \in \mathcal{R}, j \in \mathcal{A} \cup \mathcal{M}, i < j \text{ if } j \in \mathcal{M}}\right), \tag{19}$$

with  $\sigma_{\rm dist}^2$  the variance of ToF-related measurements and  $\sigma_{\rm vel}^2$  the variance of Doppler-related measurements.

#### C. Estimator

We use a standard extended Kalman filter (EKF) to estimate the true state  $s_k$  with the estimated state  $\hat{s}_k$ . The filter first predicts  $\hat{s}_k$  based on the previous state vector estimate  $\hat{s}_{k-1}$  and state covariance matrix  $P_{k-1}$  and then updates it based on the measurement  $z_k$  of snapshot k. Following [13], the prediction of state vector and state covariance matrix using the transition model (10) is defined as

$$\hat{\boldsymbol{s}}_{k}^{-} = \boldsymbol{F}_{k-1} \, \hat{\boldsymbol{s}}_{k-1} \,, \tag{20}$$

$$P_{k}^{-} = Q_{k-1} + F_{k-1} P_{k-1} F_{k-1}^{\top}.$$
 (21)

In EKF, the Kalman filter formalism is used, but with linearized functions where necessary. In our models (10) and (18), we only have to linearize the measurement function,

$$\tilde{\boldsymbol{H}}_k = \nabla_{\boldsymbol{s}} \boldsymbol{H}(\boldsymbol{s})|_{\hat{\boldsymbol{s}}_k^-} , \qquad (22)$$

where the linearization is applied at the predicted state estimate  $\hat{s}_k^-$ . Using this linearized model, we can update the state estimate based on the measurement  $z_k$ ,

$$\boldsymbol{K}_{k} = \boldsymbol{P}_{k}^{-} \, \tilde{\boldsymbol{H}}_{k}^{\top} \left[ \tilde{\boldsymbol{H}}_{k} \, \boldsymbol{P}_{k}^{-} \, \tilde{\boldsymbol{H}}_{k}^{\top} + \boldsymbol{\Sigma} \right]^{-1} , \qquad (23)$$

$$\hat{\boldsymbol{s}}_k = \hat{\boldsymbol{s}}_k^- + \boldsymbol{K}_k \left[ \boldsymbol{z}_k - \boldsymbol{H}(\hat{\boldsymbol{s}}_k^-) \right] , \qquad (24)$$

$$\boldsymbol{P}_{k} = \boldsymbol{P}_{k}^{-} + \boldsymbol{K}_{k} \left[ \tilde{\boldsymbol{H}}_{k} \boldsymbol{P}_{k}^{-} \tilde{\boldsymbol{H}}_{k}^{\top} + \boldsymbol{\Sigma} \right] \boldsymbol{K}_{k}^{\top}.$$
 (25)

The estimator is initialized by perturbing the true state to obtain the initial state estimate. For this perturbation and for the initial state covariance matrix  $P_k$  we use the process noise  $Q_k$  of the transition model (10).

When a new RP is detected during the simulation, an initial snapshot measurement leaves ambiguities, see Fig. 1. The estimator must then respect all these ambiguous possibilities and initialize the EKF multiple times and run it in parallel until this ambiguity is resolved. This resolution happens over time, either by the false estimate drifting towards the true RP over time, or by including a decision mechanism that observes the parameters of the EKF and detects when one RP estimate uncertainty becomes strongly distinct from the other and then terminates this less certain parallel EKF instance. To facilitate understanding, we show here only the tracking of the true RP and not the convergence to this RP estimate.

## III. SIMULATION

In this section, we first describe the simulation scenario and its purpose. This includes the specification of used Tx and Rx nodes and propagation environment. Additionally, we present and justify the specific parameter choices. We then present the results, analyze their underlying causes, and conclude with the implications of these results.

# A. Setup

We choose a scenario with two anchors and one mobile node. We simulate the propagation environment of a curved wall to show the usability of the previously defined method (Section II) for mapping wall geometries beyond the concept of VTs [1], [12]. The main goal of this work is to demonstrate that using Doppler information, i.e. the projected relative velocity, it is possible to track the reflection point online in a SLAM approach, simultaneously to tracking the mobile position. To demonstrate the applicability of the proposed approach to arbitrarily shaped walls, we conduct simulations on a total of five different wall geometries. For the convex and concave shapes of the wall, we choose both a circle segment shape having constant curvature and a kink shape with two sides being almost flat and a very high curvature between the sides. We also show the case of a straight wall, for which the estimation is well studied in literature [1], [4].

The mobile track is one realization of a random walk using the transition model (10), with an initial velocity in the positive x-direction, to generate a path along the wall. The RPs are then calculated using a ray tracing method to find the local minima in the ToF distance  $d_{ikj}$ , with  $i, j \in \mathcal{A} \cup \mathcal{M}$ , by minimizing over the points  $p_k$  along the wall. These minima are then the reflection points  $k \in \mathcal{R}$ , according to Fermat's principle of light choosing the shortest path [14]. Other mobile trajectories work similarly, but moving along the wall generates RPs that are well spread in the frame, see Fig. 2.

The measurement is generated by using the measurement model (18) on the true state, taking the true geometric measurement with H and then perturbing it with  $\mathcal{N}(0, \Sigma)$ . To estimate the state of the mobile and the reflection point, we use the estimator defined in (20-25) exploiting the transition model (10) and the measurement model (18). Using the same models for trajectory and measurement generation as for the estimator reduces the model mismatch to the estimation of the RP, which

in the estimator uses the transition model and in the true state is calculated exactly using the geometry of Rx, Tx and wall. This reduction in model mismatch is helpful to minimize the estimation error due to model mismatch and highlight the performance of the Doppler assisted SLAM concept and the measurement uncertainties therein.

We choose the parameters in this simulation based on a rover or pedestrian situation with low-cost UWB devices, such as the DW1000 [15] operating at  $f_c = 3.9\,\mathrm{GHz}$  with a conservative ranging error of  $\sigma_{\mathrm{dist}}^2 = 0.3\,\mathrm{m}$ . Similarly, for an initial speed of  $\dot{p} = [1.2\,\mathrm{m/s}, 0]^{\mathrm{T}}$  and dynamic mobile behavior in this order of magnitude for the simulation duration, an integration time for the Doppler measurement of  $\Delta t = 0.2\,\mathrm{s}$  is possible. According to this we also choose the simulation sampling time equivalently. This integration time is directly related to the minimal resolvable Doppler frequency of  $\Delta f_{\min} = \frac{1}{\Delta t} = 5\,\mathrm{Hz}$ . Following this, a velocity measurement error of  $\sigma_{\mathrm{vel}}^2 = 0.5\,\mathrm{m/s}$  based on (13) is chosen for this simulation. For the estimator, we choose the process noises  $\sigma_i^2 = 5\,\mathrm{m^2/s^3}$  for  $i \in \mathcal{M}$  and  $\sigma_r^2 = 25\,\mathrm{m^2/s}$  for  $r \in \mathcal{R}$ .

# B. Results

The results of this simulation are presented in Fig. 2. In general we can see that both the mobile position and the RPs can be tracked. This means that we have achieved *SLAM*, localization with respect to the mobile position and mapping with respect to the RPs and thus the wall.

Further we can see in the left column, that for convex wall shapes (top) the RPs are more concentrated compared to concave shapes (bottom), where they are more spread. Additionally we see that convex, straight and low curvature concave walls produce two RPs, one for each anchor, that exist over the whole simulation period. In contrast the stronger curved concave kink geometry, although having temporarily up to four RPs, generates appearance and disappearance events for some RPs, which can be observed well in the middle bottom frame where the distance measurements are shown. Both of these findings have geometric reasons and imply that concave walls can be mapped faster with this method, even though they might create problems due to RPs having more dynamic behaviors.

Also note that the position estimation error for the mobile path is much lower compared to the RPs, see Fig. 2 in the right column. This lower position error has several reasons. First, the state description for the mobile containing position and velocity information is more complex than the one of the RPs only containing position information. Second, the mobile position is updated in the filter using all measurement data, LoS distances, MPC distances and relative Doppler measurements. In contrast the estimation of one specific RP is only using the distance and the relative Doppler measurement of this specific MPC constituting a much smaller set of data. Third, the mobile position estimation benefits from access to direct LoS distance measurements, which offer higher fidelity. This higher fidelity is achieved, because they depend only on a single unknown—the mobile's position—whereas MPC

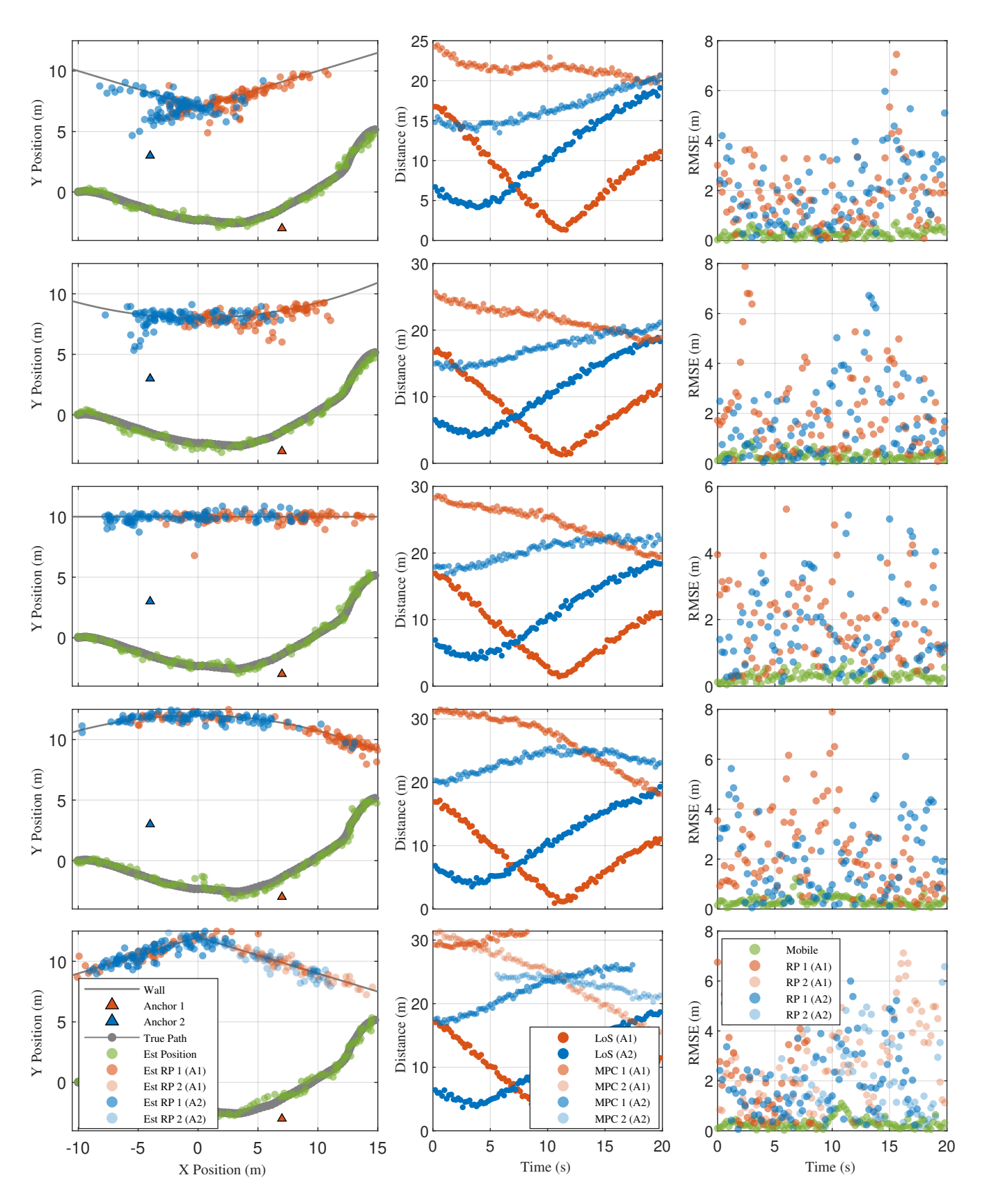


Fig. 2. On the left, the different tracking scenarios for different wall shapes are displayed. In the middle column the respective distance measurements over time are plotted, making it is easier to differentiate between the different reflection points and observe when they appear or disappear. In the right column the RMSE of each mobile and RP position estimation is shown.

measurements also rely on the estimated positions of the reflection points. In postprocessing this lack in accuracy for RP estimates can be compensated by combining the multitude of RP estimates to recover the wall shape.

Further we can observe that the RP estimation accuracy for the convex shapes seems to be lower as for the concave when looking at the left column, especially visible at the kink in the top scenario in Fig. 2. However, the RMSE does not change significantly between the different wall shape scenarios. This consistent RMSE is likely due to the MPC distance measurement having higher fidelity than the Doppler measurement due to less unknown quantities influencing it and due to the absolute measurement value being higher relative to the respective measurement standard deviation. This results in the measurement uncertainty not being circular in two dimension, but rather being stretched along the ellipse with Tx and Rx as focal points. This ellipse describes all possible RPs when only taking into account the distance measurement of a MPC, thus the more uncertain the Doppler measurement is, the less information about the angular position on this ellipse exist. Since this stretched two dimensional error bar has more overlap with the wall in concave geometries—the ellipse is tangentially touching the wall—compared to the convex cases, the error spread seems lower in this case. This effect is primarily occurring, because intuitively we assume the error of an estimated RP to be its distance to the wall and not its distance to the true respective RP.

This perceived error difference and the reasoning behind it additionally show that using the velocity information indeed provides angular information about the RP position on this ellipse albeit this information is less accurate as the ToF information defining the size of this ellipse. This angular information helps to resolve the ambiguity along the MPC ellipse for RP estimation.

## IV. CONCLUSION

This paper presented an algorithm that exploits multipath propagation for the simultaneous localization of a mobile Rx and the mapping of the corresponding RPs. The proposed method combines delay measurements with relative Doppler shifts of MPCs, providing information about both the size of the equidistant single-bounce MPC ellipse and the angular position of the RP on this ellipse. The relative Doppler shift is obtained from the phase difference between the LoS and MPCs in the received signal. By relying on relative Doppler measurements, the method eliminates the need for strict synchronization, enabling deployment with low-cost hardware, such as UWB devices.

In contrast to state-of-the-art methods that employ the concept of static VTs and strictly rely on the assumption of straight walls, the proposed approach directly estimates the positions of RPs. This direct estimation of RPs allows the mapping of environments with arbitrary wall geometries using only a single antenna at both Tx and Rx nodes. The feasibility of the method was demonstrated through simulations

incorporating delay and Doppler measurements of MPCs. The results confirm that the approach allows accurate estimation of both Rx position and RPs across a variety of wall geometries, including convex and concave surfaces. Simulations further showed that RPs on convex, straight, and low-curvature concave walls are present throughout the trajectory, with no appearance or disappearance. In contrast, in highly concave geometries, the appearance and disappearance of RPs depend on the Rx position along the trajectory.

The main result, SLAM in differently shaped environment geometries, will be useful when deploying robotic swarms for exploration in unknown environments, such as naturally formed caves or cluttered indoor spaces.

In the future, this method can be tested experimentally or through simulations with even more complex wall shapes and trajectories. This future work may require improving the estimation algorithm and extending it to merge multiple RP tracks for a unified wall estimate.

## REFERENCES

- C. Gentner, T. Jost, W. Wang, S. Zhang, A. Dammann, and U.-C. Fiebig, "Multipath assisted positioning with simultaneous localization and mapping," *IEEE Transactions on Wireless Communications*, vol. 15, no. 9, pp. 6104–6117, 2016.
- [2] E. Leitinger, F. Meyer, F. Hlawatsch, K. Witrisal, F. Tufvesson, and M. Z. Win, "A belief propagation algorithm for multipath-based SLAM," *IEEE Trans. Wireless Commun.*, vol. 18, no. 12, pp. 5613–5629, 2019.
- [3] A. Zayets and E. Steinbach, "Interpolation and extrapolation of multipath fingerprints using virtual transmitter placement," in 2018 IEEE International Conference on Communications (ICC), 2018, pp. 1–7.
- [4] H. Naseri and V. Koivunen, "Cooperative simultaneous localization and mapping by exploiting multipath propagation," *IEEE Transactions on Signal Processing*, vol. 65, no. 1, pp. 200–211, 2016.
- [5] C. Gentner, M. Ulmschneider, R. Karásek, and A. Dammann, "Simultaneous localization of a receiver and mapping of multipath generating geometry in indoor environments," in 2021 IEEE Radar Conference (RadarConf21). IEEE, 2021, pp. 1–6.
- [6] S. Zhang, F. Broghammer, E. Staudinger, R. Pöhlmann, C. Gentner, M. Schmidhammer, and A. Dammann, "Swarm navigation in lunar caves: The first proof-of-concept mission on Lanzarote," in 2025 IEEE/ION Position, Location and Navigation Symposium, PLANS 2025, April 2025. [Online]. Available: https://elib.dlr.de/212589/
- [7] J. Krška, C. Gentner, and V. Navrátil, "Angle of arrival measurements with ultra-wide band transceivers: Design and evaluation," in 2024 18th European Conference on Antennas and Propagation (EuCAP). IEEE, 2024, pp. 1–5.
- [8] M. Walter, D. Shutin, and U.-C. Fiebig, "Joint delay Doppler probability density functions for air-to-air channels," *International Journal of Antennas and Propagation*, vol. 2014, no. 1, p. 814218, 2014.
- [9] P. E. Howland, D. Maksimiuk, and G. Reitsma, "FM radio based bistatic radar," *IEE Proceedings - Radar, Sonar and Navigation*, vol. 152, no. 3, pp. 107–115, 2005.
- [10] Y. Bar-Shalom, X. R. Li, and T. Kirubarajan, Estimation with Applications to Tracking and Navigation. Wiley-Interscience, 2001.
- [11] C. Gentner and T. Jost, "Indoor positioning using time difference of arrival between multipath components," in *International conference on indoor positioning and indoor navigation*. IEEE, 2013, pp. 1–10.
- [12] M. Schmidhammer and C. Gentner, "Multipath-enhanced device-free localization using low-cost ultra-wideband devices," in 2022 16th European Conference on Antennas and Propagation (EuCAP). IEEE, 2022, pp. 1–5.
- [13] H. L. V. Trees and K. L. Bell, *Bayesian bounds for parameter estimation and nonlinear filtering/tracking*. Wiley-IEEE press, 2007.
- [14] M. Born and E. Wolf, Principles of optics: electromagnetic theory of propagation, interference and diffraction of light. Elsevier, 2013.
- [15] Decawave Ltd., DW1000 User Manual, 2017, version 2.18. [Online]. Available: https://www.qorvo.com/products/p/DW1000